Inorganic Chemistry
Cite This: Inorg. Chem. 2019, 58, 13578−13590
Forum Article
pubs.acs.org/IC

Murine Calprotectin Coordinates Mn(II) at a Hexahistidine Site with Ca(II)-Dependent Affinity

Rose C. Hadley,[†] Derek M. Gagnon,[‡] Andrew Ozarowski,[§] R. David Britt,[‡] and Elizabeth M. Nolan*[,†]

[†]Department of Chemistry, Massachusetts Institute of Technology (MIT), Cambridge, Massachusetts 02139, United States
[‡]Department of Chemistry, University of California, Davis, Davis, California 95616, United States
[§]National High Magnetic Field Laboratory, Florida State University, Tallahassee, Florida 32310, United States

Supporting Information

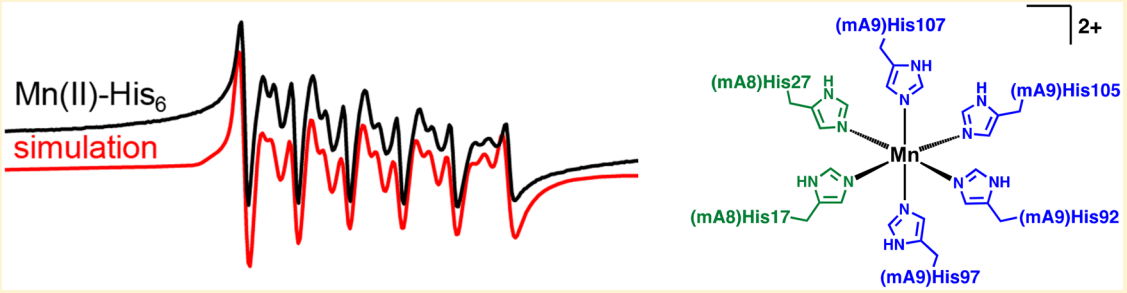

ABSTRACT: Manganese is an essential metal ion that bacterial pathogens need to acquire from the vertebrate host during infection. In the mammalian nutritional immunity strategy to combat bacterial infection, the host restricts bacterial access to Mn(II) by sequestering this metal nutrient using the protein calprotectin (CP). The role of murine calprotectin (mCP) in Mn(II) sequestration has been demonstrated in vivo, but the molecular basis of this function has not been evaluated. Herein, biochemical assays and electron paramagnetic resonance (EPR) spectroscopy are employed to characterize the Mn(II) binding properties of mCP. We report that mCP has one high-affinity Mn(II) binding site. This site is a His_6 site composed of His17 and His27 of mS100A8 and His92, His97, His105, and His107 of mS100A9. Similar to the human ortholog (hCP), Ca(II) binding to the EF-hand domains of mCP enhances the Mn(II) affinity of the protein; however, this effect requires ≈10-fold more Ca(II) than was previously observed for hCP. Mn(II) coordination to the His_6 site also promotes self-association of two mCP heterodimers to form a heterotetramer. Low-temperature X-band EPR spectroscopy revealed a nearly octahedral Mn(II) coordination sphere for the Mn(II)-His_6 site characterized by the zero-field splitting parameters D = 525 MHz and E/D = 0.3. Further electron-nuclear double resonance studies with globally ^{15}N-labeled mCP provided hyperfine couplings from the coordinating ϵ-nitrogen atoms of the His ligands (a_{iso} = 4.3 MHz) as well as the distal δ-nitrogen atoms (a_{iso} = 0.25 MHz). Mn(II) competition assays between mCP and two bacterial Mn(II) solute-binding proteins, staphylococcal MntC and streptococcal PsaA, showed that mCP outcompetes both proteins for Mn(II) under conditions of excess Ca(II). In total, this work provides the first coordination chemistry study of mCP and reveals striking similarities in the Mn(II) coordination sphere as well as notable differences in the Ca(II) sensitivity and oligomerization behavior between hCP and mCP.

INTRODUCTION

Transition metal ions are essential for many cellular processes, including regulation, catalysis, and signaling.[1] During bacterial infection, the invading pathogen must obtain metal nutrients from the host. As a result, the competition for nutrient metal ions between the host and pathogen is an important facet of the host−pathogen interaction.[1] In a process termed "nutritional immunity", the host innate immune system deploys metal-sequestering proteins to lower the levels of available metal ions at infection sites in an effort to starve the invading pathogen.[1,2]

Mn(II) sequestration is an important component of this host response to infection because many bacterial pathogens utilize Mn-containing enzymes when colonizing the host.[3−5] Mn-containing superoxide dismutases are expressed and utilized by bacterial pathogens to curb reactive-oxygen-species-mediated cell destruction.[6−8] Mn is an important cofactor for enzymes involved in central metabolism, including class Ib ribonucleotide reductase, which produces deoxyribonucleotides from ribonucelotides.[9,10] Additional metabolic enzymes, such as *Salmonella typhimurium* propionate kinase and *Escherichia coli* lactonase UlaG, have Mn(II)-dependent activity.[11,12] The Mn(II)-dependent enzyme fructose 1,6-

Special Issue: Metals in Biology: From Metallomics to Trafficking
Received: March 17, 2019
Published: May 30, 2019

DOI: 10.1021/acs.inorgchem.9b00763
Inorg. Chem. 2019, 58, 13578−13590

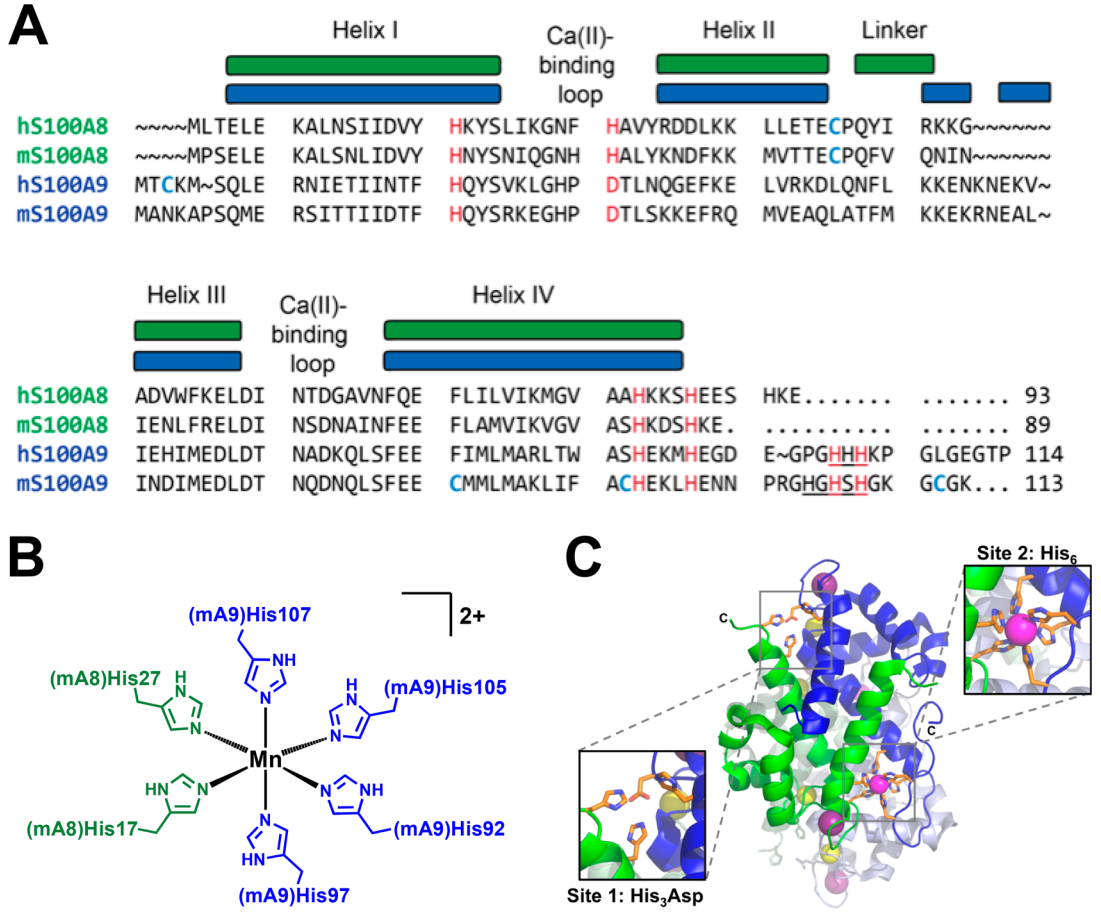

Figure 1. Overview of the primary structure and His_6 metal-binding site of mCP and the crystal structure of hCP. (A) Amino acid sequence alignment of human (h) and murine (m) S100A8 and S100A9 subunits of CP. The Ca(II)-binding regions are indicated, and the conserved transition-metal-binding residues are shown in red. Cysteine residues are shown in blue, and the portions of the S100A9 C-terminal tails containing His residues are underlined. The secondary structural elements represented are for the human subunits. (B) Predicted and experimentally determined His_6 site of mCP based on sequence alignment of the human and murine S100A8 and S100A9 subunits. A coordinated Mn(II) ion is shown. (C) Crystal structure of the Mn(II)-, Ca(II)-, and Na(I)-bound hCP heterotetramer (PDB: 4XJK).[32] One heterodimer shows the S100A8 subunit in green and the S100A9 subunit in blue, and the other heterodimer is gray. Metal ions are shown as spheres: Mn(II) is magenta, Ca(II) is yellow, and Na(I) is purple.

bis(phosphatase) II, involved in gluconeogenesis, is essential for the virulence of the intracellular pathogen *Francisella tularensis*.[13−15] Mn enzymes also contribute to antibiotic resistance. In particular, the fosfomycin-inactivating enzyme FosB in *Staphylococcus aureus* and the ATP-binding cassette (ABC)-F ATPase protein involved in antibiotic resistance in *Mycobacterium tuberculosis* utilize Mn(II) as a cofactor.[16,17] In order to obtain Mn(II), bacteria express ABC and natural resistance associated macrophage protein (NRAMP) transporters that allow the import of this nutrient.[5] For instance, the importance of staphylococcal Mn(II) import systems MntABC and MntH has been highlighted in murine models of *S. aureus* infection.[18,19] PsaABC, the Mn(II) import system in *Streptococcus pneumoniae*, is critical for infection in multiple model systems.[20] Mn(II) import systems are important for virulence in a number of other pathogens, including *Salmonella enterica* serovar Typhimurium,[8] *Bacillus anthracis*,[21] and *Enterococcus faecalis*.[22]

To date, the only known Mn(II)-sequestering host-defense protein is calprotectin (CP; S100A8/S100A9 oligomer, MRP8/MRP14 oligomer) (Figure 1).[23] The role of CP in biology and infectious disease has been illuminated through many studies involving mouse models in which $S100A9^{-/-}$ (CP-deficient) mice are utilized.[8,24−29] In 2008, murine CP (mCP) was shown to reduce Mn(II) levels and limit *S. aureus* growth in murine abscesses.[25] This seminal work provided the first evidence for the ability of CP to sequester Mn(II) and inspired biochemical and biophysical investigations into the Mn(II)-binding properties of the protein.[7,30−34] Nevertheless, current understanding of the metal-binding properties of CP is almost exclusively based on the evaluation of hCP, the human form of the protein.[23]

hCP is a heterooligomer of the S100 proteins S100A8 (10.8 kDa) and S100A9 (13.2 kDa). Each subunit contains two Ca(II)-binding sites: one C-terminal canonical EF-hand and one N-terminal noncanonical EF-hand.[35] In the absence of Ca(II) ions, hCP exists as a heterodimer.[36] Ca(II) binding to the EF-hand domains causes the self-association of two heterodimers to form a heterotetramer.[37−39] Each hCP heterodimer contains two distinct transition-metal-binding sites that form at the S100A8/S100A9 interface: a His_3Asp site (site 1) and a His_6 site (site 2) (Figure 1).[23] In the current working model, hCP is released from immune or epithelial cells at infection sites, where it encounters high (~2 mM) extracellular Ca(II) levels and forms a heterotetramer.[23,39,40] Tetramerization enhances the transition-metal-ion affinities

DOI: 10.1021/acs.inorgchem.9b00763
Inorg. Chem. 2019, 58, 13578−13590

and protease stability of hCP.[23,39,41] Biochemical, structural, and spectroscopic studies of Mn(II) coordination by hCP has provided a comprehensive molecular description of how the protein sequesters Mn(II).[30−34] Importantly, hCP employs a biologically unprecedented hexahistidine (His_6) motif to sequester Mn(II), and the presence of excess Ca(II) ions lowers the apparent dissociation constant ($K_{d1,Mn(II)}$) by at least 3 orders of magnitude.[30−34] On the basis of all available data, Ca(II)-bound hCP coordinates Mn(II) with subnanomolar affinity at the His_6 site.[34] The His_3Asp site, in contrast, has relatively low affinity for Mn(II) in the absence and presence of Ca(II) ions [micromolar K_d assigned by room-temperature electron paramagnetic resonance (EPR) spectroscopy in the presence of excess Ca(II) ions].[30] Thus, the His_3Asp site binds Mn(II) but lacks the ability to sequester it.

Given the importance and broad application of murine models in studying the biological function of CP, understanding the metal-binding properties of mCP is necessary. Amino acid sequence alignment reveals similarities and differences between the human and murine S100A8 and S100A9 subunits. The alignment indicates that the residues that compose sites 1 and 2 are conserved (Figure 1A), which suggests that hCP and mCP exhibit similar metal-binding properties and provides a working hypothesis that mCP employs a high-affinity His_6 motif to sequester divalent transition-metal ions, including Mn(II). Nevertheless, hCP and mCP share only ∼56% amino acid identity, a lower value compared to the average of 85% amino acid identity between human and murine polypeptides.[42] This relatively large variability in the primary structures suggests that there may be some important structural and functional differences between the human and murine orthologs that warrant careful examination. Toward addressing the current knowledge gap about mCP, we recently reported the initial biochemical characterization of the protein, which demonstrated that, similar to hCP, apo mCP exists as a mS100A8/mS100A9 heterodimer and that Ca(II)-binding results in the self-association of two heterodimers to form a heterotetramer.[43] However, ∼10-fold more Ca(II) equivalents were required to completely tetramerize mCP compared to hCP even though the two proteins exhibit similar Ca(II)-binding regions (Figure 1A). To the best of our knowledge, this observation provided the first experimental indication that the biophysical properties of hCP and mCP differ, and we reason that additional studies are warranted to further evaluate this possibility and elucidate whether there are functional consequences. Pertinent to the current study, our preliminary evaluation of the metal-binding ability of mCP demonstrated that mCP coordinates a number of transition metal ions, including Mn, present in a complex bacterial growth medium.[43]

In this work, we investigate the Mn(II)-binding properties of mCP. We report that mCP coordinates Mn(II) at a high-affinity His_6 site and displays Ca(II)-dependent Mn(II) affinity at this site, and that Mn(II) binding at the His_6 site confers tetramerization in the absence of Ca(II) ions. We also demonstrate that mCP can outcompete the solute-binding proteins (SBPs) staphylococcal MntC and streptococcal PsaA for Mn(II) under conditions of high Ca(II). These Mn(II)-binding studies are consistent with the role of mCP in Mn(II) sequestration in the host−pathogen interaction, as expected based on prior work that involved animal models of infection. Lastly, the current work reveals an important similarity in the Mn(II)-binding capability between hCP and mCP: the His_6 site, which is a significant contributor during the battle between the host and pathogen for nutrient metal ions as well as additional differences in the Ca(II)-dependent behavior.

RESULTS AND DISCUSSION

Preparation and Biochemical Characterization of mCP Metal-Binding Site Variants. We first designed protein variants to probe the amino acid residues in mS100A8 and mS100A9 predicted to be important for Mn(II) binding. Because the metal-binding-site residues are conserved in hCP and mCP, we prepared and characterized mCP variants with mutations that disrupted either the putative His_3Asp site [ΔHis_3Asp; mS100A8(H83A)(H87A)/mS100A9(H21A)-(D31A)] or four residues of the putative His_6 site [ΔHis_4; mS100A8(H17A)(H27A)/mS100A9(H92A)(H97A)] (Figure 1 and Table S1). The C-terminal tail of mS100A9 contains an HXHXH motif spanning residues 103−107. To evaluate whether these His residues contribute to Mn(II) binding, we prepared variants with one or two His → Ala mutations in this region (Tables 1 and S1 and S2). Following overexpression of each subunit in *E. coli* and reconstitution of the mCP heterodimers according to a reported protocol,[43] the variants were characterized by inductively coupled plasma mass spectrometry (ICP-MS), sodium dodecyl sulfate polyacrylamide gel electrophoresis (SDS-PAGE), liquid chromatography−mass spectrometry (LC−MS), circular dichroism (CD) spectroscopy, and analytical size-exclusion chromatography (SEC) (Tables S3−S6 and Figures S1−S3). ICP-MS and SDS-PAGE analyses indicated that the proteins were isolated in the apo form (Tables S4 and S5) and in high purity (Figure S1), respectively. LC−MS analysis demonstrated that the mS100A8 subunits displayed partial loss of the initiator methionine, whereas mS100A9 subunits lacked this residue (Table S3). Cleavage of Met1 is a common post-translational modification observed during heterologous overexpression in *E. coli*.[44] All variants afforded CD spectra consistent with an α-helical fold in the presence and absence of Ca(II) (Figure S2). Lastly, analytical SEC established that the purified proteins were isolated as heterodimers, as indicated by elution volumes of 12.0−12.1 mL (Table S6 and Figure S3). In the presence of excess Ca(II) ions in the running buffer, the peak for each variant displayed a shift to a lower elution volume (11.3−11.4 mL), indicating Ca(II)-induced tetramerization (Table S6 and Figure S3). This behavior is consistent with our prior characterization of mCP.[43]

Table 1. mS100A9 C-Terminal Tail Variants

mCP variant	tail residues (101−109)
mCP	RGHGHSHGK
(H103A)	RGAGHSHGK
(H105A)	RGHGASHGK
(H107A)	RGHGHSAGK
(H103A)(H105A)	RGAGASHGK
(H103A)(H107A)	RGAGHSAGK
(H105A)(H107A)	RGHGASAGK

Analytical SEC Uncovers the His_6 Site and Mn(II)-Induced Tetramerization of mCP. Guided by our initial studies of Mn(II) binding to hCP,[30,31] we first incubated mCP (100 μM) with 10 equiv of Mn(II) and analyzed the sample by SEC at pH 7.0. In the absence of Mn(II), mCP exhibits a single peak that elutes at 12.1 min (Figure 2A). The presence

DOI: 10.1021/acs.inorgchem.9b00763
Inorg. Chem. 2019, 58, 13578−13590

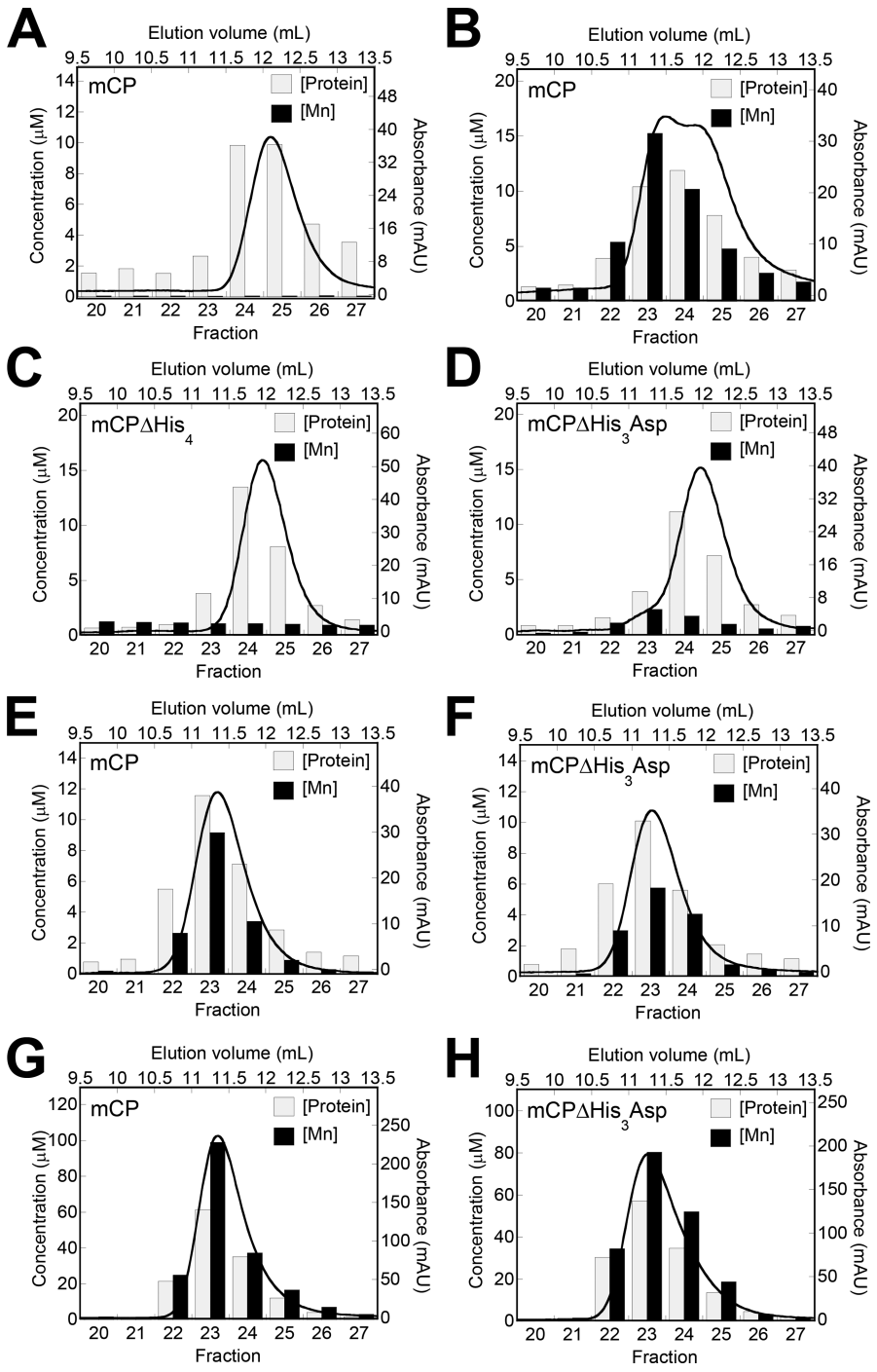

Figure 2. Representative data demonstrating Mn retention by mCP and variants following SEC. Each plot shows a representative SEC chromatogram (black trace) and the quantification of protein and Mn concentrations in the collected fractions (bars). For experiments in the absence of added Ca(II), the protein concentration was either 100 μM (A–D) or 500 μM (G and H). For experiments in the presence of 25 mM Ca(II), the protein concentration was 100 μM (E and F). The samples were incubated without (A) or with Mn(II) (B–H). For samples containing Mn(II), the Mn(II) concentration was 1 mM (B–D), 100 μM (D and E; +Ca(II) samples), or 5 mM (G and H). The elution buffer was 75 mM HEPES, 100 mM NaCl, 200 μM TCEP, pH 7.0 and T = 4 °C.

of Mn(II) caused the peak to broaden and exhibit two local maxima at 11.5 and 11.8 min (Figure 2B). Quantitation of protein and Mn(II) concentrations in the fractions by optical absorption spectroscopy (A_{280}) and ICP-MS, respectively, revealed negligible Mn(II) in the apo sample, as expected. In contrast, ∼1 equiv of Mn(II) was retained over the course of elution of the +Mn(II) sample. Thus, in the absence of Ca(II) ions, mCP coordinates Mn(II) with sufficiently high affinity to retain the metal during elution. The Mn(II)-induced peak shift to lower elution volume also indicates that Mn(II) binding to mCP induces tetramerization, behavior previously observed for hCP.[30,31]

We extended this experiment to examine the ability of the ΔHis_3Asp and ΔHis_4 variants to retain Mn(II). When we employed 100 μM protein and 10 equiv of Mn(II), both proteins displayed peak elution volumes consistent with

DOI: 10.1021/acs.inorgchem.9b00763
Inorg. Chem. 2019, 58, 13578–13590

heterodimers, and negligible Mn(II) retention was observed (Figure 2C,D). The result for ΔHis_4 was consistent with our working hypothesis that mCP uses a high-affinity His_6 site to coordinate Mn(II). In contrast, the results with ΔHis_3Asp were unexpected. Because Ca(II) ions enhanced the Mn(II) affinity of hCP, we questioned whether ΔHis_3Asp retains Mn(II) when excess Ca(II) is present. Thus, we examined samples of mCP and ΔHis_3Asp (100 μM) containing 1 equiv of Mn(II) using an elution buffer supplemented with 25 mM Ca(II) (Figure 2E,F). Under these conditions, the peaks for both mCP and ΔHis_3Asp displayed a shift to a lower elution volume, corresponding to tetramerization, and both proteins retained substoichiometric Mn(II). Next, we repeated the SEC experiments with mCP and ΔHis_3Asp in the absence of Ca(II) ions using a 5-fold higher protein concentration (500 μM) and 10 equiv of Mn(II) (Figure 2G,H). Under these conditions, both proteins displayed comparable peak elution volume shifts consistent with nearly complete tetramerization, and both proteins retained Mn(II). Taken together, these results indicate that (i) Mn(II)-induced tetramerization of mCP exhibits a protein-concentration dependence, (ii) mutation of the His_3Asp residues compromises the ability of the protein to retain Mn(II) at site 2 and display Mn(II)-dependent self-association, and (iii) the Mn(II) affinity is enhanced by Ca(II) binding to the EF-hand domains. We also note that ΔHis_3Asp displayed a greater increase in the α-helicity upon Ca(II) addition compared to mCP and the other variants (Figure S2), further suggesting that the ΔHis_3Asp mutations impact protein structure.

Because the four residues of the putative His_6 site are essential for Mn(II) retention during elution from the SEC column, we next examined the contribution of H103, H105, and H107 in the mS100A9 C-terminal tail (Figure 3). For mCP(H103A), we observed a similar behavior as mCP with Mn(II) retention and partial tetramerization when the protein (100 μM) was incubated with 10 equiv Mn(II) prior to elution from the SEC column (Figure 3A). In contrast, under these same experimental conditions, mCP(H105A) and mCP(H107A) eluted as heterodimers with negligible Mn(II) retained (Figure 3B,C). These results indicate that H105 and H107 are involved in Mn(II) coordination and that H103 does not participate in Mn(II) binding. Thus, these initial SEC experiments indicate that mCP employs a His_6 site composed of His17 and His27 of mS100A8 and His92, His97, His105 and His107 of mS100A9 to coordinate Mn(II) (Figure 1B). These residues are conserved in mCP and hCP. Moreover, this site is the high-affinity site and appears to display Ca(II)-dependent Mn(II) affinity.

Mn(II) Competition Studies Demonstrate That Ca(II) Ions Enhance the Mn(II) Affinity of mCP. On the basis of our prior studies of hCP, which demonstrated that Ca(II) ions enhance the transition-metal affinities of the His_3Asp and His_6 sites,[30,39] and our preliminary biochemical evaluation of mCP,[43] we hypothesized that mCP displays similar Ca(II)-dependent behavior. In this prior work on hCP, we performed Zinpyr-1 (ZP1) competition assays to examine Ca(II)-dependent Mn(II) binding to the protein.[30,31] ZP1 is a Ca(II)-independent fluorescent sensor with two di-2-picolylamine-based metal-binding sites that exhibits fluorescence quenching upon Mn(II) binding ($K_{d1,Mn(II)}$ = 550 nM).[45] When we combined ZP1 (1 μM), mCP (4 μM), and Mn(II) (4 μM), the fluorescence from ZP1 was quenched, indicating that Mn(II) was bound to the sensor and not mCP (Figure 4).

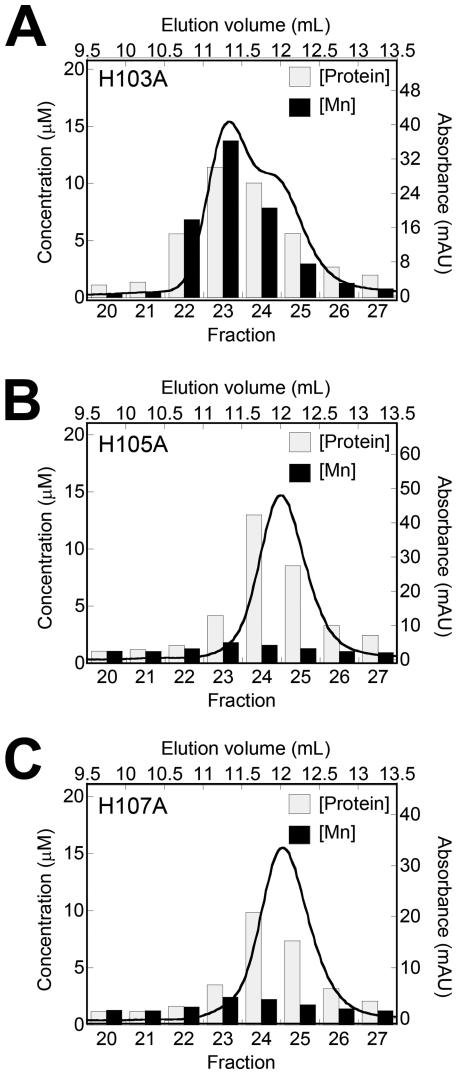

Figure 3. Representative data demonstrating Mn retention by mCP C-terminal tail variants following SEC. Each plot shows a representative SEC chromatogram (black trace) and the quantification of protein and Mn concentrations in the collected fractions (bars). The variants (100 μM) H103A (A), H105A (B), and H107A (C) were incubated with Mn(II) (1 mM) in the absence of added Ca(II). The elution buffer was 75 mM HEPES, 100 mM NaCl, 200 μM TCEP, pH 7.0 and T = 4 °C.

This behavior is consistent with that of hCP.[30] Upon titration of Ca(II) into this solution, the fluorescence of ZP1 increased and reached its maximum emission once >200 equiv of Ca(II) relative to mCP were added. In agreement with previous reports, maximum ZP1 emission occurred following the addition of ~20 equiv of Ca(II) to mixtures of ZP1, hCP-Ser [hS100A8(C42S)/hS100A9(C3S) variant], and Mn(II) (Figure 4).[30] These results show that the Mn(II) affinity of mCP is Ca(II)-dependent and that mCP is able to outcompete ZP1 for Mn(II) when excess Ca(II) ions are present, indicating that mCP binds Mn(II) with $K_{d1,Mn(II)}$ < 550 nM under conditions of high Ca(II). The requirement of >200 equiv of Ca(II) to fully enhance the Mn(II) affinity is consistent with our prior report on mCP that showed that >200 equiv of Ca(II) was necessary for complete tetramerization.[43] We also note that the sigmoidal titration curve for mCP indicates that cooperativity is at play, the origin and details of which are a

DOI: 10.1021/acs.inorgchem.9b00763
Inorg. Chem. 2019, 58, 13578−13590

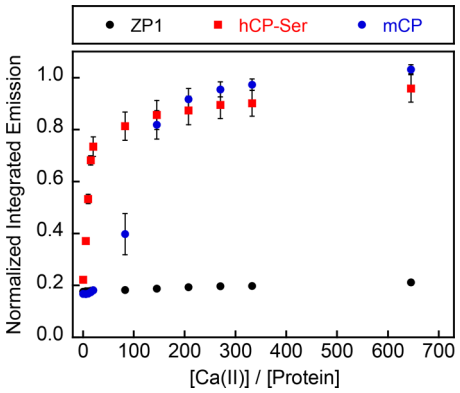

Figure 4. Titration of Ca(II) into a mixture of ZP1 (1 μM), hCP-Ser or mCP (4 μM), and Mn(II) (4 μM) monitored by fluorescence spectroscopy. The integrated emission was normalized to the integrated emission from the apo sensor (average ± SEM; n = 3). The buffer was 75 mM HEPES, 100 mM NaCl, 200 μM TCEP, pH 7.0 and T = 25 °C.

subject for future work. Lastly, the Ca(II) responses of hCP and mCP clearly differ, which may have implications for the working model of mCP action. Along these lines, the total extracellular Ca(II) concentration is ≈2 mM and mCP subunits are reported to reach concentrations on the order of hundreds of micromolar at the infection sites.[40,46] Taken together with the current data, these [Ca(II)]/[mCP] ratios present the possibility that the speciation of mCP in the extracellular space may include mixtures of heterodimers and heterotetramers. Nevertheless, it is also possible that the 2 mM value for total extracellular Ca(II) does not accurately estimate the Ca(II) concentrations that mCP encounters at the infection sites. Recent laser-ablation ICP-MS studies of infected murine tissues revealed that Ca localizes to neutrophils and mCP, and although not quantified, the Ca concentration at these locales is higher than that in the surrounding tissues.[28]

Mn(II) Competition Studies Further Define the His_6 Site. We next evaluated how many equiv of Mn(II) mCP binds with high affinity. We performed Mn(II) competition titrations between ZP1 (1 μM) and mCP or variant (4 μM) in the presence of 300 equiv of Ca(II) (1.2 mM). Titration of Mn(II) into the ZP1/mCP/Ca(II) mixture resulted in no change in ZP1 fluorescence until a ≈1:1 [Mn(II)]/[protein] ratio was achieved, further demonstrating that mCP binds 1 equiv of Mn(II) with greater affinity than ZP1 (Figure 5A). The ΔHis_3Asp variant also outcompeted ZP1 for ≈1 equiv of Mn(II), whereas the ΔHis_4 variant was unable to compete with ZP1 for this metal ion. Moreover, the mS100A9 C-terminal tail variants H105A and H107A afforded titration curves indicative of Mn(II) competition and reduced Mn(II) affinity compared to mCP and ΔHis_3Asp (Figure 5B). The H103A variant, in contrast, outcompeted ZP1. Taken together, these results are in agreement with the observations from the SEC experiments and show that mCP coordinates 1 equiv of Mn(II) with high affinity at the His_6 site that is completed by residues H105 and H107 of the mS100A9 C-terminal tail.

EPR Spectroscopy of Mn(II)-Bound mCP. To further characterize the Mn(II)-His_6 site of mCP and describe its electronic structure, we applied multifrequency EPR spectroscopic methods. First, we examined the X-band EPR spectra of Mn(II)-bound mCP and several variants (ΔHis_3Asp, H103A, H105A, and H107A) analyzed in the biochemical experiments described above. We also studied mCP-Ser, an all Cys → Ser variant that we previously reported (Figure S4).[43] Guided by our prior EPR spectroscopic evaluation of the human ortholog[30−32] and the Mn(II)-binding studies of mCP presented in this work, we prepared EPR samples containing 200 μM protein, 0.9 equiv of Mn(II), and 300 equiv of Ca(II). Under these high Ca(II) conditions, we expected that all of the Mn(II) will be bound to the His_6 site with negligible free Mn(II) in solution.

The continuous-wave (CW) X-band EPR spectrum of Mn(II) bound to the His_6 site of mCP is typical for the high-spin Mn(II) d^5 ion (Figure 6). The isotropic g value of 2.0008 is typical for the spherical symmetry of the electron distribution. The magnitude of the g value is remarkably similar to the value of 2.001 that was determined for Mn(II)- and Ca(II)-bound hCP-Ser.[32] The sextet features centered around g = 2.0008 result from the hyperfine interaction with the ^{55}Mn nucleus ($I = {}^5/_2$, 100% abundance). This observed sextet arises from m_s transitions in the "inner" $m_s = \pm{}^1/_2$ Kramer's doublet. Hyperfine splitting in the "outer" Kramer's doublet ($m_s = \pm{}^1/_2 \leftrightarrow \pm{}^3/_2 \leftrightarrow \pm{}^5/_2$) is rarely resolved in

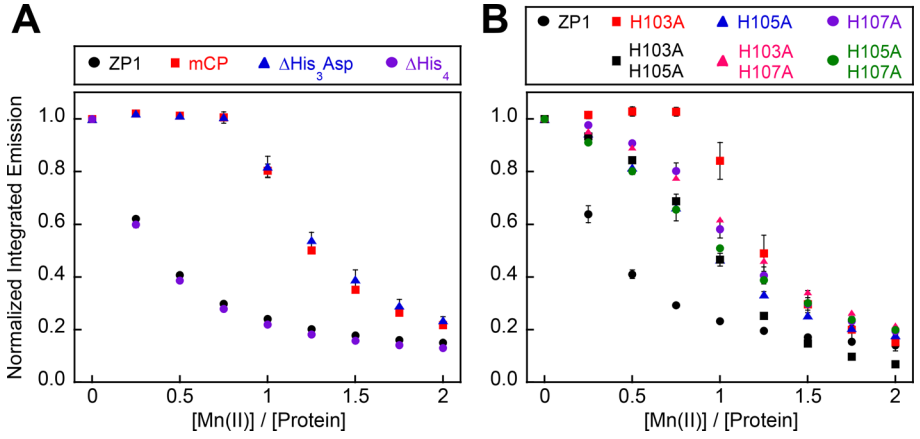

Figure 5. Titration of Mn(II) into a mixture of ZP1 (1 μM), mCP or variant (4 μM), and Ca(II) (1.2 mM) monitored by fluorescence spectroscopy. Data for mCP, ΔHis_3Asp, and ΔHis_4 (A) and mS100A9 C-terminal tail variants (B). The integrated emission was normalized to the integrated emission from the apo sensor (average ± SEM; $n \geq 3$). The buffer was 75 mM HEPES, 100 mM NaCl, 200 μM TCEP, pH 7.0 and T = 25 °C. In the legend, "ZP1" refers to a sample containing ZP1 and no protein.

DOI: 10.1021/acs.inorgchem.9b00763
Inorg. Chem. 2019, 58, 13578−13590

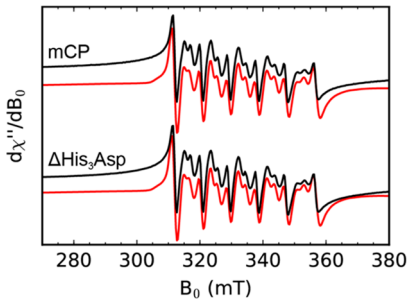

Figure 6. X-band EPR spectra (black) and simulations (red) for Mn(II)- and Ca(II)-bound mCP and ΔHis_3Asp. The buffer was 75 mM HEPES, 100 mM NaCl, pH 7.5.

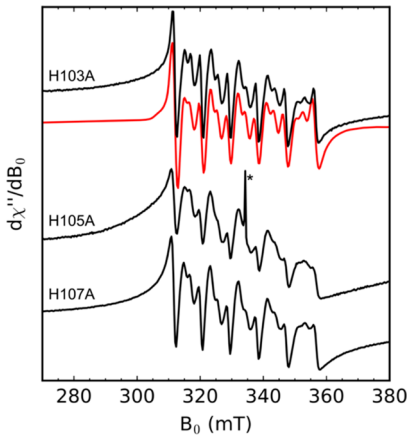

Figure 7. X-band EPR spectra (black) of Mn(II)- and Ca(II)-bound mCP variants H103A, H105A, and H107A. The red trace for H103A is a simulation using the parameters determined for Mn(II)- and Ca(II)-bound mCP. The peak marked by an asterisk is a background quartz radical. The buffer was 75 mM HEPES, 100 mM NaCl, pH 7.5.

frozen spectra because of orientation-dependent broadening.[47,48] The magnitude of this hyperfine interaction, 248 MHz, is nearly identical to the 247 MHz value measured for Mn(II)- and Ca(II)-bound hCP-Ser and consistent with the decrease in the ^{55}Mn hyperfine interaction observed with increasing imidazole concentration.[32,49] Between each sextet pair are two additional transitions. These transitions arise from formally forbidden $\Delta m_s \pm 1$ and $\Delta m_I \pm 1$ transitions. At higher frequencies, the intensities of these transitions diminish, which further confirms their identities as forbidden transitions (Figures S5 and S6). The intensities and positions of these transitions are indicative of the magnitude of the zero-field-splitting (ZFS) parameters D and E/D. Simulations of the X-band EPR spectrum of Mn(II)- and Ca(II)-bound mCP utilizing *EasySpin*[50] afforded values of 525 MHz and 0.30 for D and E/D, respectively (Figure 6, red trace). The low ZFS is indicative of a highly symmetric, octahedral coordination sphere. The values are remarkably similar to the simulated D and E/D values of 485 MHz and 0.30 determined for Mn(II)- and Ca(II)-bound hCP-Ser.[32]

We employed the same protein/Mn(II)/Ca(II) ratio to prepare samples of the mCP variants and found that Mn(II)- and Ca(II)-bound ΔHis_3Asp exhibits the same EPR spectrum as mCP (Figure 6) and can be simulated using identical parameters (Figure 6, red trace), supporting the conclusion that substoichiometric Mn(II) is only bound at the His_6 site. Moreover, the EPR spectrum of Mn(II)- and Ca(II)-bound mCP-Ser could also be simulated with the same parameters (Figure S4), indicating that the Cys → Ser mutations have a negligible effect on Mn(II) binding at the His_6 site. We attempted to make EPR samples of the ΔHis_4 variant, but precipitation occurred during the sample preparation, so we did not analyze the samples. The mCP variants with mutations in the mS100A9 C-terminal tail afforded EPR spectra consistent with H105 and H107 completing the Mn(II)-His_6 coordination sphere but not H103 (Figure 7). H103A showed no change in the EPR spectrum compared to mCP (Figure 6) and can be simulated using parameters identical to those of mCP (Figure 7, red trace). In contrast, H105A and H107A show markedly perturbed EPR spectra compared to the spectra for mCP and H103A (Figures 6 and 7). The large increase in the intensity of the forbidden transitions relative to the allowed transitions indicates that the symmetry of the Mn(II) site is lowered. Along these lines, our prior EPR spectroscopic study of Mn(II)-bound variants of hCP-Ser revealed that analogous mutations in the C-terminal tail resulted in a coordination sphere that included solvent-derived ligands, which reduced the symmetry,[32] and we reason that a similar situation occurs with the H105A and H107A variants of mCP.

To more quantitatively measure the interaction of the Mn(II) ion with the histidine residues of the His_6 site of mCP, we prepared globally ^{15}N-labeled protein (^{15}N-mCP) for electron-nuclear double resonance (ENDOR) spectroscopy.[51−53] This sample contained ^{15}N-mCP (200 μM), 0.9 equiv of Mn(II), and 300 equiv of Ca(II). The Mims ENDOR spectrum of Mn(II)- and Ca(II)-bound ^{15}N-mCP displays two sets of resonances centered at the ^{15}N Larmor frequency (Figure 8). The broader doublet (labeled A in Figure 8) is

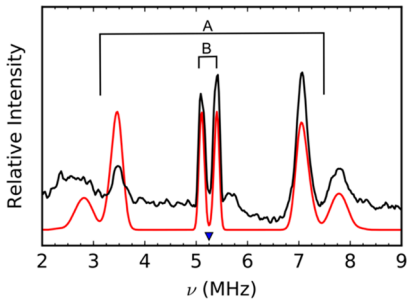

Figure 8. ^{15}N Mims ENDOR spectrum (black) of Mn(II) and Ca(II) bound to globally labeled ^{15}N-mCP. The red trace is a simulation. The τ value is 700 ns. Spectra collected with additional τ values are presented in Figure S7. A and B indicate the two sets of resonances centered at the ^{15}N Larmor frequency. The inverted triangle indicates the ^{15}N Larmor frequency. The buffer was 75 mM HEPES, 100 mM NaCl, pH 7.5. Experimental settings: MW frequency = 34.0 GHz; field = 1216.6 mT; T = 10 K.

assigned to the proximal nitrogen atoms of the histidine imidazoles [Nε2, based on the structures of Mn(II)-bound hCP-Ser].[32,33] The splitting of the peaks is caused by a τ-dependent blind spot confirmed by collecting the spectrum with different τ values (Figure S7). This doublet can be simulated with a hyperfine tensor of [3.3, 3.6, 6.0] MHz and a_{iso} of 4.3 MHz. The isotropic hyperfine coupling (a_{iso}) is nearly identical with the 4.36 MHz measured for Nε2 of hCP-Ser.[32] The second, narrower doublet (labeled B in Figure 8) is assigned to the distal nitrogen atoms of the histidine

DOI: 10.1021/acs.inorgchem.9b00763
Inorg. Chem. 2019, 58, 13578−13590

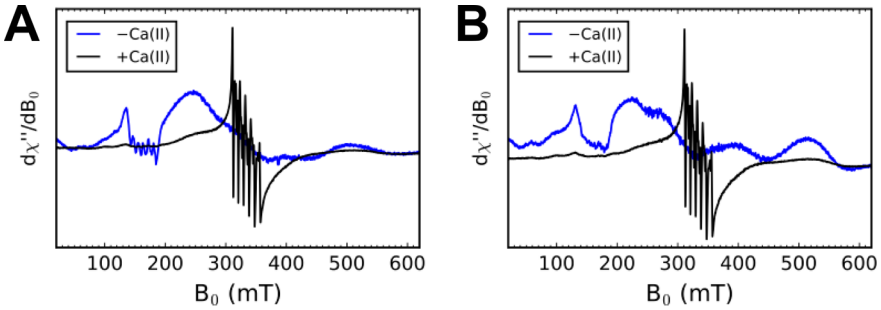

Figure 9. X-band EPR spectra of 500 μM mCP, 500 μM Mn(II), and 500 μM MntC (A) or PsaA (B) without or with 60 mM Ca(II) following a 14 h incubation at room temperature. The buffer was 75 mM HEPES, 100 mM NaCl, pH 7.5.

imidazoles (Nδ1). This doublet can be simulated with an isotropic hyperfine coupling constant of 0.25 MHz. Consistent with the CW results comparing Mn(II)- and Ca(II)-bound mCP with hCP-Ser, this value is nearly identical with the 0.24 MHz measured for hCP-Ser.[32] The approximately 18 times difference in the isotropic nitrogen hyperfine value of the ε and δ nitrogen atoms is consistent with the observed trend for other histidine-coordinated metal ions.[51−53]

In summary, a comparison of these EPR spectroscopic data for Mn(II)- and Ca(II)-bound mCP with those previously analyzed for the human ortholog reveals that the electronic structure of the Mn(II) ion coordinated to the His_6 site is remarkably similar in both proteins. In particular, for samples prepared such that only the His_6 site is occupied with Mn(II), the ^{55}Mn hyperfine parameters, ZFS values, and g values for Mn(II)- and Ca(II)-bound mCP are nearly identical with the parameters previously reported for Mn(II)- and Ca(II)-bound hCP-Ser.[32]

mCP Can Outcompete MntC and PsaA for Mn(II). The bacterial pathogens *S. aureus* and *S. pneumoniae* employ the ABC transporters MntABC and PsaABC, respectively, to import Mn(II).[54,55] MntC and PsaA are the SBPs responsible for capturing extracellular Mn(II) and delivering it to MntB and PsaC, respectively. We recently demonstrated that hCP-Ser can outcompete MntC and PsaA for Mn(II) under conditions of high Ca(II).[34] To evaluate whether mCP exhibits similar behavior, we prepared samples containing a 1:1:1 ratio of mCP, SBP, and Mn(II) (500 μM each) in the absence and presence of 120 equiv of Ca(II) and evaluated the Mn(II) speciation in the samples by X-band EPR spectroscopy. As described previously, the EPR spectroscopic signatures of Mn(II)-bound hCP-Ser and SBPs are distinct.[34] In contrast to the six-line feature centered at $g \approx 2$ for Mn(II)- and Ca(II)-bound hCP-Ser, the Mn(II)-bound SBPs present a broad, relatively featureless spectrum at ca. $g = 2$ and sharp spectral features in the $g \approx 4.5$ region.[34] Similar to our observations for hCP-Ser, this Mn(II) speciation analysis revealed that mCP outcompetes MntC and PsaA for Mn(II) under conditions of excess Ca(II) but not in the absence of this cation (Figure 9). On the basis of the reported $K_{d,Mn(II)}$ values of MntC and PsaA ($K_{d,Mn(II)} \approx 4$[56] and ≤ 10 nM,[57] respectively), these observations indicate that Ca(II)-bound mCP binds Mn(II) with a subnanomolar K_d value. We also note that these results complement prior biological work. In a murine model of infection, deletion of MntABC was detrimental to the ability of *S. aureus* to cause infection in mice expressing mCP, which suggested that mCP competes with MntABC for Mn(II).[18]

Comparisons of hCP and mCP. The current studies examine the molecular basis of Mn(II) sequestration by mCP. This work is important because CP is the only known Mn(II)-sequestering host protein, and the vast majority of biochemical and biophysical characterization reported to date has focused on the human ortholog, whereas an understanding of the biological function of this protein is largely derived from murine infection models.[23] This current biochemical and EPR spectroscopic investigation demonstrates that the Mn(II)-binding properties of mCP are remarkably similar to those of hCP. In particular, both proteins bind 1 equiv of Mn(II) with high affinity at a His_6 site that is formed by four His residues that reside at the S100A8/S100A9 dimer interface and two His residues in an HXH motif of the S100A9 C-terminal tail. EPR spectroscopic analyses reveal that Mn(II) binding to mCP occurs in a highly symmetric coordination sphere with parameters very similar to those determined previously for hCP. Moreover, both proteins show enhanced Mn(II) affinities in the presence of excess Ca(II) ions, Mn(II)-induced tetramerization in the absence of Ca(II), and the ability to outcompete two bacterial SBPs for this metal ion.

Despite these similarities, there are also notable differences in the Mn(II)-binding properties of hCP and mCP. In particular, how Ca(II) modulates the biophysical properties of the two proteins differs; mCP requires ≈10-fold more Ca(II) than hCP to exhibit complete conversion to the heterotetramer and fully enhanced Mn(II) affinity at the His_6 site. Ca(II) ions are an important component of the working model for the extracellular function of CP in metal withholding because Ca(II) binding induces tetramerization, enhances the transition-metal affinities and antibacterial activity, and protects the protein from proteolytic degradation.[23] Further biophysical and biological work is needed to illuminate both the origins and impacts of the differing Ca(II) sensitivities of hCP and mCP. The higher Ca(II) requirement of mCP suggests that it may exhibit different speciation in the extracellular space where the Ca(II) concentration is ≈2 mM,[40] possibly with a higher proportion of heterodimers compared to hCP. Along similar lines, we also observed reduced tetramerization of mCP in the presence of excess Mn(II) compared to prior studies of hCP, which further indicates that the self-association properties of the hCP and mCP heterodimers vary. Taken together, these observations suggest that local and/or global differences in the protein structures and/or dynamics exist, which warrant further investigation.

CONCLUSION

In closing, this work provides a foundation for understanding the molecular basis for Mn(II) sequestration by mCP in murine models of infection as well as further examining the

DOI: 10.1021/acs.inorgchem.9b00763
Inorg. Chem. 2019, 58, 13578−13590

coordination chemistry and function of the His_6 site of this protein. Whether the conserved His_6 metal-binding motif that both mice and humans utilize in the metal-withholding innate immune response is a feature present in a wider range of CP orthologs remains to be investigated. Ultimately, this work helps to bridge the gap between the molecular and physiological studies of CP and emphasizes the importance of investigating and appreciating both the similarities and differences in human and murine host-defense strategies.

EXPERIMENTAL SECTION

General Materials and Methods. All chemicals were purchased from commercial suppliers and used as received. Milli-Q (18.2 MΩ·cm) water was used in the preparation of all buffers and metal-ion solutions. Buffers used for the biochemical and spectroscopic experiments were prepared from ULTROL-grade HEPES (CalBiochem) and TraceSELECT NaCl (MilliporeSigma) to limit metal-ion contamination from buffer components and stored in polypropylene containers. Calcium-containing buffers for analytical SEC were prepared with $CaCl_2{\cdot}2H_2O$ (>99.0%, MilliporeSigma). All buffers were filtered (0.2 μm) before use. Stock solutions of Ca(II) (1 M, 100 mL) were prepared from $CaCl_2{\cdot}2H_2O$ (>99.0%, MilliporeSigma) in acid-washed volumetric glassware and stored in polypropylene tubes. Stock solutions of Mn(II) (1 M, 100 mL) were prepared from $MnCl_2{\cdot}4H_2O$ (99.999%, Alfa Aesar) in acid-washed volumetric glassware and stored in polypropylene tubes. Working solutions of metal ions were prepared daily by dilution in Milli-Q water and stored in polypropylene tubes. Protein aliquots were stored at −80 °C and thawed only once prior to use. All protein concentrations were determined using calculated extinction coefficients (https://web.expasy.org/protparam/). All CP concentrations are for the heterodimer form of mCP (mS100A8/mS100A9; ε_{280} = 5960 M^{-1} cm^{-1}) or hCP-Ser (hS100A8/hS100A9; ε_{280} = 18450 M^{-1} cm^{-1}). Reported equivalents of Mn(II) and Ca(II) are relative to the CP heterodimer. MntC (ε_{280} = 35870 M^{-1} cm^{-1}) and PsaA (ε_{280} = 35870 M^{-1} cm^{-1}) are monomers, and concentrations of these proteins are for the monomer.

Design of Synthetic Genes. The synthetic genes containing the nucleotide sequences of mS100A8 and mS100A9 and all variants were ligated into the *Nde*I and *Xho*I restriction sites of the pET41a vector, as described previously.[43] Synthetic genes for mS100A8(H17A)-(H27A), mS100A8(H83A)(H87A), mS100A9(H21A)(D31A), and mS100A9(H92A)(H97A) were codon-optimized for *E. coli* expression, synthesized, and ligated into the *Nde*I and *Xho*I restriction sites of pET41a vectors by ATUM (formerly DNA2.0). The nucleotide sequences are provided in the Supporting Information. Each plasmid was transformed into chemically competent *E. coli* TOP10 cells, isolated using a miniprep kit (Qiagen), and analyzed by DNA sequencing (Quintara Biosciences). The pET41a vectors containing the mS100A9(H103A), mS100A9(H105A), mS100A9(H107A), mS100A9(H103A)(H105A), mS100A9(H103A)(H107A), and mS100A9(H105A)(H107A) genes were prepared by site-directed mutagenesis as described below.

Site-Directed Mutagenesis. The His → Ala point mutations in the mS100A9 gene were prepared by site-directed mutagenesis using the primer pairs and templates listed in Table S2. The oligonucleotide primers were synthesized by Integrated DNA Technologies (Coralville, IA). A modified Quick-Change site-directed mutagenesis protocol was employed to generate the variants using Pfu Turbo DNA polymerase (Agilent). The PCR protocol was 95 °C for 30 s, 95 °C for 30 s, 60−66 °C for 1 min (Table S2), 68 °C for 12 min (25 times), and 4 °C hold temperature. *Dpn*I (New England Biolabs) was used to degrade the template plasmid. A 0.75 μL aliquot was added to the sample and incubated at 37 °C for 3 h. At 1.5 h into the incubation, a supplemental 0.75 μL aliquot of *Dpn*I was added. The remaining plasmid DNA was transformed into chemically competent *E. coli* TOP10 cells, and the resulting plasmids were isolated using a miniprep kit (Qiagen) and analyzed by DNA sequencing (Quintara Biosciences).

Protein Overexpression and Purification. mCP and variants were overexpressed and purified as described previously.[43] MntC and PsaA were overexpressed and purified as described previously.[34] hCP-Ser was also overexpressed and purified as described previously.[39] The globally ^{15}N-labeled mS100A8 and mS100A9 subunits were overexpressed using reported procedures for the hCP-Ser subunits.[32] In brief, a M9 minimal medium (2 L) for overexpression was prepared with $^{15}NH_4Cl$ as the nitrogen source. Immediately before use, 1 mL of a 1000x vitamin mix (400 mg of choline chloride, 500 mg of folic acid, 1.1 g of pantothenic acid, 500 mg of nicotinamide, 500 mg of myoinositol, 500 mg of pyridoxal·HCl, 500 mg of thiamine·HCl, and 50 mg of riboflavin in 15 mL of Milli-Q water) was added to 2 L shaker flasks containing 1 L of the M9 minimal medium along with a few flakes each of $FeCl_3$ (MilliporeSigma), biotin (Alfa Aesar), and thiamine·HCl (MilliporeSigma). Next, kanamycin was added to 50 μg mL^{-1}. A 20 mL aliquot of a saturated culture of BL21(DE3) cells containing either pET41a-*mS100A8* or pET41a-*mS100A9* grown in LB medium was pelleted and resuspended in the M9 minimal medium (25 mL). The centrifugation and resuspension steps were repeated, and the resulting cell suspensions were used to inoculate the culture media for overexpression of each subunit. The overexpression was performed as described previously for mCP, with induction at OD_{600} ≈ 0.6.[43] The ^{15}N-labeled protein was reconstituted and purified as described previously for mCP.[43] The protein yields were in the range ≈14−60 mg per 2 L of culture for mCP and all variants, including ^{15}N-labeled protein.

Analytical SEC. A GE ÄKTA Purifier FPLC System housed in a cold room (4 °C) and outfitted with a Superdex 75 10/300 GL SEC column was used for all analytical SEC. The elution buffer was 75 mM HEPES, 100 mM NaCl, 200 μM TCEP, pH 7.0, ±25 mM Ca(II). Mn(II) (500 μM or 5 mM) was added to samples from a 1 M stock solution, and the samples were incubated at room temperature for at least 15 min prior to SEC analysis. The column was calibrated with blue dextran and a low-molecular-weight protein mixture (GE Healthcare Life Sciences) consisting of ribonuclease A (13.7 kDa), carbonic anhydrase (29 kDa), ovalbumin (44 kDa), and conalbumin (75 kDa) prior to use (Table S6). Proteins were buffer-exchanged (3 times) into the running buffer using an Amicon spin filter (0.5 mL, 10 kDa MWCO). Samples (100 μM, 300 μL) were prepared and loaded into a 100 μL injection loop, and the FLPC system was programmed to load 500 μL of solution through the injection loop (sample + elution buffer) onto the column. The samples were eluted over one column volume (24 mL) at a flow rate of 0.5 mL min^{-1}. At least two independent replicates were performed for each experiment, and representative data from one experiment are shown. The protein concentration of each collected fraction was determined by absorbance at 280 nm in acid-washed quartz cuvettes using a Beckman DU 800 UV−vis spectrophotometer equipped with a Peltier thermostat. To prepare ICP-MS samples for total Mn analyses, an aliquot (50 μL) of each fraction was diluted to 2 mL with 5% nitric acid (TraceSELECT, Fluka) and supplemented with a 2 ppb Tb internal standard.

LC−MS. An Agilent 6545 series Q-TOF LC−MS system with an Agilent Eclipse plus C18 with (2.1 × 50 mm, 1.8 μm particle size) was used for all analyses. Each protein was diluted in Milli-Q water to a final concentration of ≈10 μM. A 5 or 10 μL protein aliquot was injected into the column, and each sample was eluted using a gradient of 25−75% B over 10 min with a flow rate of 0.3 mL min^{-1} (solvent A, 0.1% formic acid in water; solvent B, 0.1% formic acid in acetonitrile). The spectra were deconvoluted using the maximum entropy algorithm in the *MassHunter Bioconfirm* software (Agilent).

ICP-MS. The metal content of the protein samples was determined using an Agilent 7900 ICP-MS spectrometer with an autosampler housed in the Center for Environmental Health Sciences Bioanalytical Core Facility at MIT. The instrument was used in helium mode. Calibration standards were prepared from a serial dilution of the Environmental Standard calibration mixture (Agilent, part 5183-4688). The standards and samples were spiked with a 2 ppb Tb (100

DOI: 10.1021/acs.inorgchem.9b00763
Inorg. Chem. 2019, 58, 13578−13590

ppb stock in 5% nitric acid) internal standard (Agilent, part 5190-8590). Sample volumes of either 1.7 or 2.0 mL were employed.

CD Spectroscopy. CD spectra were collected using a Jasco J-500 spectrometer housed in the Biophysical Instrumentation Facility at MIT. Proteins were buffer-exchanged into the CD buffer (1 mM Tris-HCl at pH 7.5 and 1 mM DTT) prior to analysis. For samples containing Ca(II), an aliquot was added to the sample from a 1 M Ca(II) stock solution to afford 3 mM Ca(II) in the sample. Samples (10 μM, 300 μL) were transferred to a Hellma quartz cuvette (1 mm path length) for analysis. Spectra were collected from 195 to 260 nm using a continuous scan mode (50 nm min^{-1}) and a 1 nm bandwidth. Reported spectra are averages of triplicate baseline-subtracted scans.

Fluorescence Titrations. ZP1 was synthesized as described previously[58] and kindly provided by Dr. Jacob Goldberg and Prof. Stephen J. Lippard. Stock solutions of ZP1 (≈3 mM) were prepared in anhydrous dimethyl sulfoxide, aliquoted, and stored at −20 °C. Each aliquot was thawed only once. Titrations were performed in 75 mM HEPES, 100 mM NaCl, 200 μM TCEP, pH 7.0. Mn(II) competition titrations between ZP1 and mCP (or variant) were performed as described previously for hCP.[30] In brief, aliquots of protein were thawed and subsequently buffer-exchanged into 75 mM HEPES, 100 mM NaCl, 200 μM TCEP, pH 7.0 using 0.5 mL Amicon spin filters (10 kDa MWCO). For each titration, a 2 mL solution of titration buffer containing ZP1 (1 μM) and protein (4 μM) was prepared in a 1 cm pathlength nitric acid-washed quartz cuvette. Ca(II) (1.2 mM) was added from a 1 M stock solution (2.4 μL). The mixture was titrated with Mn(II) (2 or 4 μL of a 500 μM Mn(II) solution). After each Mn(II) addition, the solution was gently mixed and incubated for ≈10 min at room temperature and in the dark prior to recording of the fluorescence emission spectrum. For the Ca(II) titration, protein (4 μM) and Mn(II) (4 μM) were preincubated for ≈10 min prior to titration of Ca(II) [2 μL additions of either 20 or 250 mM Ca(II)] into the sample.

Emission spectra were collected on a Photon Technologies International QuantaMaster 40 fluorimeter outfitted with a CW xenon source for excitation, autocalibrated QuadraScopic monochromators, a multimode PMT detector, and a circulating water bath maintained at 25 °C. This instrument was controlled by the *FelixGX* software package. The excitation wavelength was 490 nm. The emission spectra were collected and integrated over 500−650 nm.

EPR Spectroscopy. To prepare mCP samples for EPR spectroscopy, all protein aliquots were buffer-exchanged into 75 mM HEPES and 100 mM NaCl at pH 7.5. For X-band EPR spectroscopy, 200 μM protein was prepared with 180 μM Mn(II) (0.9 equiv) in the absence or presence of 60 mM Ca(II) (300 equiv). Samples (500 μL) were incubated for at least 15 min prior to being frozen in liquid nitrogen. Most protein samples were shipped in a liquid-nitrogen dewar to the CalEPR facility at University of California, Davis for analysis. For 388 GHz EPR spectroscopy, a sample (500 μL) of mCP (500 μM) was incubated with Ca(II) (50 mM) and Mn(II) (450 μM) for at least 15 min, transferred to a 1 mL LDPE vial (Fisher Scientific), frozen in liquid nitrogen, and shipped on dry ice to the National High Magnetic Field Laboratory (Tallahassee, FL) for analysis. To evaluate the competition for Mn(II) between mCP and SBPs, mixed samples of SBP and mCP were prepared as described previously,[34] with the exception that the +Ca(II) samples contained 60 mM Ca(II). A 1:1 Mn(II)/SBP sample (1 mM each) was prepared along with an mCP sample (1 mM) that contained Ca(II) (120 mM). Following ≈15 min of incubation, aliquots of each solution were mixed by pipette in a 1:1 ratio and incubated for ≈14 h at room temperature. The samples (170 μL) were subsequently frozen in liquid nitrogen and stored at −80 °C prior to analysis at MIT using instrumentation in the Department of Chemistry Instrumentation Facility.

At CalEPR, CW X-band (ca. 9.38 GHz) EPR spectra were collected on a Bruker ELEXSYS E500 CW EPR spectrometer with a superhigh QE (SHQE) resonator and an Oxford Instruments ESR900 liquid-helium cryostat. Spectra were collected under slow-passage conditions so as not to distort the line shape. The spectrometer conversion time was set to 80 ms and a data point collected every ≈0.3 mT with the 0.5 mT modulation amplitude at 100 kHz. Spectra were collected at a temperature of 10 K with 0.2 mW of microwave power.

At CalEPR, Q-band (ca. 34.1 GHz) spectra were collected on a Bruker ELEXSYS E580 X/Q-band pulse EPR spectrometer equipped with an Oxford Instrument CF935 liquid-helium cryostat and a home-built probe.[59] Field sweeps were acquired using a two-pulse Hahn echo sequence ($\pi/2-\tau-\pi-\tau-$echo) with a two-step phase-cycling program, and data were collected every 0.3 mT. ^{15}N ENDOR spectra were collected using the Mims ENDOR sequence ($\pi/2-\tau-\pi/2-\pi_{RF}-\pi/2-\tau-$echo).[60] The 50 μs long π_{RF} pulse was amplified using an ENI A1000 amplifier providing 1 kW of peak power. The amplified radio-frequency (RF) pulse was utilized without attenuation before the sample. The shot repetition time was 1 ms at 10 K for all pulse sequences.

At the National High Magnetic Field Laboratory, the transmission spectrometer was utilized to obtain a 388 GHz field sweep of Mn(II)-mCP in the presence of excess Ca(II).[61] The temperature was 30 K with a modulation amplitude of 0.5 mT at 50 kHz and a downfield sweep rate of 0.50 mT s^{-1}.

At MIT, X-band EPR spectral investigations of the Mn(II) competition between mCP and SBPs were performed on a Bruker EMXplus spectrometer equipped with an ER4119HS resonator and a ColdEdge Technologies 4K waveguide cryogen-free cryostat. The spectrometer conversion time was set to 7.2 ms, and a data point was collected every ≈0.1 mT with 0.5 mT modulation amplitude at 100 kHz. Spectra were collected at 10 K.

EPR Data Analysis. All spectra were simulated in *Matlab R2017a* (The Mathworks, Inc., Novi, MI) using the freely available *EasySpin* toolbox.[50] The field-swept EPR spectrum can be interpreted using the phenomenological spin Hamiltonian:

$$H = \frac{\beta_e}{h}\mathbf{B}\cdot g\cdot S + a_{iso}S\cdot I + D[S_z^2 - S(S+1)/3] + E(S_x^2 - S_y^2) \quad (1)$$

The terms in the Hamiltonian are the electron Zeeman interaction with an applied static magnetic field **B**, the isotropic hyperfine interaction (a_{iso}) of the unpaired electrons with the ^{55}Mn nucleus, the nuclear Zeeman interaction I, the axial ZFS tensor D, and the rhombic ZFS term E for the high-spin Mn(II) ion ($S = {}^5/_2$). β_e is the Bohr magneton, g is the electron g factor, and h is the Planck constant. An example code for the simulation of the field sweeps and an expanded discussion on how the simulations were performed are provided in the Supporting Information. The simulation procedure was adapted from prior work.[32]

The ^{15}N ENDOR spectra can be interpreted with a simplified phenomenological spin Hamiltonian.[62,63]

$$H = \beta_e\mathbf{B}\cdot g\cdot S/h + \sum_i (S\cdot\mathbf{A}_i\cdot I_i - \beta_n g_{n,i}\mathbf{B}\cdot I_i) \quad (2)$$

The ZFS and ^{55}Mn hyperfine interaction are ignored, and the system is treated as a pseudo $S = {}^1/_2$ spin system. Here, $\mathbf{A}_i$ corresponds to the electron nuclear hyperfine interaction tensor for atom i, β_n is the nuclear magneton, $g_{n,i}$ is the nuclear g factor for atom i, and other terms are as defined above for eq 1. An expanded discussion of the simulation is provided in the Supporting Information. The approximation used for the simulations was adapted from prior work.[32]

■ ASSOCIATED CONTENT

Supporting Information

The Supporting Information is available free of charge on the ACS Publications website at DOI: 10.1021/acs.inorgchem.9b00763.

Design of the synthetic genes, Tables S1−S6, and Figures S1−S7 (PDF)

DOI: 10.1021/acs.inorgchem.9b00763
Inorg. Chem. 2019, 58, 13578−13590

AUTHOR INFORMATION

Corresponding Author

*E-mail: lnolan@mit.edu. Phone: 617-452-2495.

ORCID

Derek M. Gagnon: 0000-0003-1737-6365
Andrew Ozarowski: 0000-0001-6225-9796
R. David Britt: 0000-0003-0889-8436
Elizabeth M. Nolan: 0000-0002-6153-8803

Notes

The authors declare no competing financial interest.

ACKNOWLEDGMENTS

We gratefully acknowledge NIH Grants R01GM118695 (to E.M.N.) and R35GM126961 (to R.D.B.) for financial support. ICP-MS instrumentation is housed in the MIT Center for Environmental Health Sciences Bioanalytical Core, which is supported by NIH Grant P30-ES002109. The MIT Biophysical Instrumentation Facility for the Study of Complex Macromolecular Systems is supported by NSF Grant 0070319. A portion of this work was performed at the National High Magnetic Field Laboratory, which is supported by the National Science Foundation Cooperative Agreement DMR-1644779 and the State of Florida. The Q-TOF mass spectrometer is housed in the MIT Department of Chemistry Instrumentation Facility.

REFERENCES

(1) Hood, M. I.; Skaar, E. P. Nutritional immunity: transition metals at the pathogen–host interface. *Nat. Rev. Microbiol.* **2012**, *10* (8), 525–537.

(2) Weinberg, E. D. Nutritional immunity: Host's attempt to withhold iron from microbial invaders. *J. Am. Med. Assoc.* **1975**, *231* (1), 39–41.

(3) Juttukonda, L. J.; Skaar, E. P. Manganese homeostasis and utilization in pathogenic bacteria. *Mol. Microbiol.* **2015**, *97* (2), 216–228.

(4) Brophy, M. B.; Nolan, E. M. Manganese and microbial pathogenesis: sequestration by the mammalian immune system and utilization by microorganisms. *ACS Chem. Biol.* **2015**, *10* (3), 641–651.

(5) Papp-Wallace, K. M.; Maguire, M. E. Manganese transport and the role of manganese in virulence. *Annu. Rev. Microbiol.* **2006**, *60*, 187–209.

(6) Garcia, Y. M.; Barwinska-Sendra, A.; Tarrant, E.; Skaar, E. P.; Waldron, K. J.; Kehl-Fie, T. E. A superoxide dismutase capable of functioning with iron or manganese promotes the resistance of *Staphylococcus aureus* to calprotectin and nutritional immunity. *PLoS Pathog.* **2017**, *13* (1), No. e1006125.

(7) Kehl-Fie, T. E.; Chitayat, S.; Hood, M. I.; Damo, S.; Restrepo, N.; Garcia, C.; Munro, K. A.; Chazin, W. J.; Skaar, E. P. Nutrient metal sequestration by calprotectin inhibits bacterial superoxide defense, enhancing neutrophil killing of *Staphylococcus aureus*. *Cell Host Microbe* **2011**, *10* (2), 158–164.

(8) Diaz-Ochoa, V. E.; Lam, D.; Lee, C. S.; Klaus, S.; Behnsen, J.; Liu, J. Z.; Chim, N.; Nuccio, S.-P.; Rathi, S. G.; Mastroianni, J. R.; Edwards, R. A.; Jacobo, C. M.; Cerasi, M.; Battistoni, A.; Ouellette, A. J.; Goulding, C. W.; Chazin, W. J.; Skaar, E. P.; Raffatellu, M. *Salmonella* mitigates oxidative stress and thrives in the inflamed gut by evading calprotectin-mediated manganese sequestration. *Cell Host Microbe* **2016**, *19* (6), 814–825.

(9) Makhlynets, O.; Boal, A. K.; Rhodes, D. V.; Kitten, T.; Rosenzweig, A. C.; Stubbe, J. *Streptococcus sanguinis* class Ib ribonucleotide reductase: high activity with both iron and manganese cofactors and structural insights. *J. Biol. Chem.* **2014**, *289* (9), 6259–6272.

(10) Rhodes, D. V.; Crump, K. E.; Makhlynets, O.; Snyder, M.; Ge, X.; Xu, P.; Stubbe, J.; Kitten, T. Genetic characterization and role in virulence of the ribonucleotide reductases of *Streptococcus sanguinis*. *J. Biol. Chem.* **2014**, *289* (9), 6273–6287.

(11) Chittori, S.; Simanshu, D. K.; Banerjee, S.; Murthy, A. M. V.; Mathivanan, S.; Savithri, H. S.; Murthy, M. R. N. Mechanistic features of *Salmonella typhimurium* propionate kinase (TdcD): insights from kinetic and crystallographic studies. *Biochim. Biophys. Acta Proteins Proteomics* **2013**, *1834* (10), 2036–2044.

(12) Garces, F.; Fernández, F. J.; Montellà, C.; Penya-Soler, E.; Prohens, R.; Aguilar, J.; Baldomà, L.; Coll, M.; Badia, J.; Vega, M. C. Molecular architecture of the Mn^{2+}-dependent lactonase UlaG reveals an RNase-like metallo-β-lactamase fold and a novel quaternary structure. *J. Mol. Biol.* **2010**, *398* (5), 715–729.

(13) Brissac, T.; Ziveri, J.; Ramond, E.; Tros, F.; Kock, S.; Dupuis, M.; Brillet, M.; Barel, M.; Peyriga, L.; Cahoreau, E.; Charbit, A. Gluconeogenesis, an essential metabolic pathway for pathogenic *Francisella*. *Mol. Microbiol.* **2015**, *98* (3), 518–534.

(14) Gutka, H. J.; Wolf, N. M.; Bondoc, J. M. G.; Movahedzadeh, F. Enzymatic characterization of fructose 1,6-bisphosphatase II from *Francisella tularensis*, an essential enzyme for pathogenesis. *Appl. Biochem. Biotechnol.* **2017**, *183* (4), 1439–1454.

(15) Kadzhaev, K.; Zingmark, C.; Golovliov, I.; Bolanowski, M.; Shen, H.; Conlan, W.; Sjöstedt, A. Identification of genes contributing to the virulence of *Francisella tularensis* SCHU S4 in a mouse intradermal infection model. *PLoS One* **2009**, *4* (5), No. e5463.

(16) Thompson, M. K.; Keithly, M. E.; Goodman, M. C.; Hammer, N. D.; Cook, P. D.; Jagessar, K. L.; Harp, J.; Skaar, E. P.; Armstrong, R. N. Structure and function of the genomically encoded fosfomycin resistance enzyme, FosB, from *Staphylococcus aureus*. *Biochemistry* **2014**, *53* (4), 755–765.

(17) Daniel, J.; Abraham, L.; Martin, A.; Pablo, X.; Reyes, S. Rv2477c is an antibiotic-sensitive manganese-dependent ABC-F ATPase in *Mycobacterium tuberculosis*. *Biochem. Biophys. Res. Commun.* **2018**, *495* (1), 35–40.

(18) Kehl-Fie, T. E.; Zhang, Y.; Moore, J. L.; Farrand, A. J.; Hood, M. I.; Rathi, S.; Chazin, W. J.; Caprioli, R. M.; Skaar, E. P. MntABC and MntH contribute to systemic *Staphylococcus aureus* infection by competing with calprotectin for nutrient manganese. *Infect. Immun.* **2013**, *81* (9), 3395–3405.

(19) Handke, L. D.; Gribenko, A. V.; Timofeyeva, Y.; Scully, I. L.; Anderson, A. S. MntC-dependent manganese transport is essential for *Staphylococcus aureus* oxidative stress resistance and virulence. *mSphere* **2018**, *3* (4), e00336-18.

(20) Marra, A.; Lawson, S.; Asundi, J. S.; Brigham, D.; Hromockyj, A. E. *In vivo* characterization of the *psa* genes from *Streptococcus pneumoniae* in multiple models of infection. *Microbiology* **2002**, *148*, 1483–1491.

(21) Gat, O.; Mendelson, I.; Chitlaru, T.; Ariel, N.; Altboum, Z.; Levy, H.; Weiss, S.; Grosfeld, H.; Cohen, S.; Shafferman, A. The solute-binding component of a putative Mn(II) ABC transporter (MntA) is a novel *Bacillus anthracis* virulence determinant. *Mol. Microbiol.* **2005**, *58* (2), 533–551.

(22) Colomer-Winter, C.; Flores-Mireles, A. L.; Baker, S. P.; Frank, K. L.; Lynch, A. J. L.; Hultgren, S. J.; Kitten, T.; Lemos, J. A. Manganese acquisition is essential for virulence of *Enterococcus faecalis*. *PLoS Pathog.* **2018**, *14* (9), No. e1007102.

(23) Zygiel, E. M.; Nolan, E. M. Transition metal sequestration by the host-defense protein calprotectin. *Annu. Rev. Biochem.* **2018**, *87*, 621–643.

(24) Hobbs, J. A. R.; May, R.; Tanousis, K.; McNeill, E.; Mathies, M.; Gebhardt, C.; Henderson, R.; Robinson, M. J.; Hogg, N. Myeloid cell function in MRP-14 (S100A9) null mice. *Mol. Cell. Biol.* **2003**, *23* (7), 2564–2576.

(25) Corbin, B. D.; Seeley, E. H.; Raab, A.; Feldmann, J.; Miller, M. R.; Torres, V. J.; Anderson, K. L.; Dattilo, B. M.; Dunman, P. M.; Gerads, R.; Caprioli, R. M.; Nacken, W.; Chazin, W. J.; Skaar, E. P. Metal chelation and inhibition of bacterial growth in tissue abscesses. *Science* **2008**, *319*, 962–965.

DOI: 10.1021/acs.inorgchem.9b00763
Inorg. Chem. 2019, 58, 13578–13590

(26) Liu, J. Z.; Jellbauer, S.; Poe, A. J.; Ton, V.; Pesciaroli, M.; Kehl-Fie, T. E.; Restrepo, N. A.; Hosking, M. P.; Edwards, R. A.; Battistoni, A.; Pasquali, P.; Lane, T. E.; Chazin, W. J.; Vogl, T.; Roth, J.; Skaar, E. P.; Raffatellu, M. Zinc sequestration by the neutrophil protein calprotectin enhances *Salmonella* growth in the inflamed gut. *Cell Host Microbe* **2012**, *11* (3), 227−239.
(27) Hood, M. I.; Mortensen, B. L.; Moore, J. L.; Zhang, Y.; Kehl-Fie, T. E.; Sugitani, N.; Chazin, W. J.; Caprioli, R. M.; Skaar, E. P. Identification of an *Acinetobacter baumannii* zinc acquisition system that facilitates resistance to calprotectin-mediated zinc sequestration. *PLoS Pathog.* **2012**, *8* (12), No. e1003068.
(28) Juttukonda, L. J.; Berends, E. T. M.; Zackular, J. P.; Moore, J. L.; Stier, M. T.; Zhang, Y.; Schmitz, J. E.; Beavers, W. N.; Wijers, C. D.; Gilston, B. A.; Kehl-Fie, T. E.; Atkinson, J.; Washington, M. K.; Peebles, R. S.; Chazin, W. J.; Torres, V. J.; Caprioli, R. M.; Skaar, E. P. Dietary manganese promotes staphylococcal infection of the heart. *Cell Host Microbe* **2017**, *22* (4), 531−542.
(29) Besold, A. N.; Gilston, B. A.; Radin, J. N.; Ramsoomair, C.; Culbertson, E. M.; Li, C. X.; Cormack, B. P.; Chazin, W. J.; Kehl-Fie, T. E.; Culotta, V. C. The role of calprotectin in withholding zinc and copper from *Candida albicans*. *Infect. Immun.* **2018**, *86* (2), e00779−17.
(30) Hayden, J. A.; Brophy, M. B.; Cunden, L. S.; Nolan, E. M. High-affinity manganese coordination by human calprotectin is calcium-dependent and requires the histidine-rich site formed at the dimer interface. *J. Am. Chem. Soc.* **2013**, *135* (2), 775−787.
(31) Brophy, M. B.; Nakashige, T. G.; Gaillard, A.; Nolan, E. M. Contributions of the S100A9 C-terminal tail to high-affinity Mn(II) chelation by the host-defense protein human calprotectin. *J. Am. Chem. Soc.* **2013**, *135* (47), 17804−17817.
(32) Gagnon, D. M.; Brophy, M. B.; Bowman, S. E. J.; Stich, T. A.; Drennan, C. L.; Britt, R. D.; Nolan, E. M. Manganese binding properties of human calprotectin under conditions of high and low calcium: X-ray crystallographic and advanced electron paramagnetic resonance spectroscopic analysis. *J. Am. Chem. Soc.* **2015**, *137* (8), 3004−3016.
(33) Damo, S. M.; Kehl-Fie, T. E.; Sugitani, N.; Holt, M. E.; Rathi, S.; Murphy, W. J.; Zhang, Y.; Betz, C.; Hench, L.; Fritz, G.; Skaar, E. P.; Chazin, W. J. Molecular basis for manganese sequestration by calprotectin and roles in the innate immune response to invading bacterial pathogens. *Proc. Natl. Acad. Sci. U. S. A.* **2013**, *110* (10), 3841−3846.
(34) Hadley, R. C.; Gagnon, D. M.; Brophy, M. B.; Gu, Y.; Nakashige, T. G.; Britt, R. D.; Nolan, E. M. Biochemical and spectroscopic observation of Mn(II) sequestration from bacterial Mn(II) transport machinery by calprotectin. *J. Am. Chem. Soc.* **2018**, *140* (1), 110−113.
(35) Gifford, J. L.; Walsh, M. P.; Vogel, H. J. Structures and metal-ion-binding properties of the Ca^{2+}-binding helix-loop-helix EF-hand motifs. *Biochem. J.* **2007**, *405* (2), 199−221.
(36) Hunter, M. J.; Chazin, W. J. High level expression and dimer characterization of the S100 EF-hand proteins, migration inhibitory factor-related proteins 8 and 14. *J. Biol. Chem.* **1998**, *273* (20), 12427−12435.
(37) Vogl, T.; Roth, J.; Sorg, C.; Hillenkamp, F.; Strupat, K. Calcium-induced noncovalently linked tetramers of MRP8 and MRP14 detected by ultraviolet matrix-assisted laser desorption/ionization mass spectrometry. *J. Am. Soc. Mass Spectrom.* **1999**, *10* (11), 1124−1130.
(38) Korndörfer, I. P.; Brueckner, F.; Skerra, A. The crystal structure of the human $(S100A8/S100A9)_2$ heterotetramer, calprotectin, illustrates how conformational changes of interacting α-helices can determine specific association of two EF-hand proteins. *J. Mol. Biol.* **2007**, *370* (5), 887−898.
(39) Brophy, M. B.; Hayden, J. A.; Nolan, E. M. Calcium ion gradients modulate the zinc affinity and antibacterial activity of human calprotectin. *J. Am. Chem. Soc.* **2012**, *134* (43), 18089−18100.
(40) Brini, M.; Ottolini, D.; Cali, T.; Carafoli, E. Calcium in health and disease. *Met. Ions Life Sci.* **2013**, *13*, 81−137.
(41) Stephan, J. R.; Nolan, E. M. Calcium-induced tetramerization and zinc chelation shield human calprotectin from degradation by host and bacterial extracellular proteases. *Chem. Sci.* **2016**, *7* (3), 1962−1975.
(42) Makałowski, W.; Zhang, J.; Boguski, M. S. Comparative analysis of 1196 orthologous mouse and human full-length mRNA and protein sequences. *Genome Res.* **1996**, *6* (9), 846−857.
(43) Hadley, R. C.; Gu, Y.; Nolan, E. M. Initial biochemical and functional evaluation of murine calprotectin reveals Ca(II)-dependence and its ability to chelate multiple nutrient transition metal ions. *Biochemistry* **2018**, *57* (19), 2846−2856.
(44) Bradshaw, R. A.; Brickey, W. W.; Walker, K. W. N-Terminal processing: the methionine aminopeptidase and N^{α}-acetyl transferase families. *Trends Biochem. Sci.* **1998**, *23* (7), 263−267.
(45) You, Y.; Tomat, E.; Hwang, K.; Atanasijevic, T.; Nam, W.; Jasanoff, A. P.; Lippard, S. J. Manganese displacement from Zinpyr-1 allows zinc detection by fluorescence microscopy and magnetic resonance imaging. *Chem. Commun.* **2010**, *46* (23), 4139−4141.
(46) Kocher, M.; Kenny, P. A.; Farram, E.; Abdul Majid, K. B.; Finlay-Jones, J. J.; Geczy, C. L. Functional chemotactic factor CP-10 and MRP-14 are abundant in murine abscesses. *Infect. Immun.* **1996**, *64* (4), 1342−1350.
(47) Duboc, C.; Phoeung, T.; Zein, S.; Pécaut, J.; Collomb, M.-N.; Neese, F. Origin of the zero-field splitting in mononuclear octahedral dihalide Mn^{II} complexes: an investigation by multifrequency high-field electron paramagnetic resonance and density functional theory. *Inorg. Chem.* **2007**, *46* (12), 4905−4916.
(48) Duboc, C.; Collomb, M.-N.; Neese, F. Understanding the zero-field splitting of mononuclear manganese(II) complexes from combined EPR spectroscopy and quantum chemistry. *Appl. Magn. Reson.* **2010**, *37*, 229−245.
(49) Un, S. Structure and nature of manganese(II) imidazole complexes in frozen aqueous solutions. *Inorg. Chem.* **2013**, *52* (7), 3803−3813.
(50) Stoll, S.; Schweiger, A. EasySpin, a comprehensive software package for spectral simulation and analysis in EPR. *J. Magn. Reson.* **2006**, *178* (1), 42−55.
(51) Mims, W. B.; Peisach, J. The nuclear modulation effect in electron spin echoes for complexes of Cu^{2+} and imidazole with ^{14}N and ^{15}N. *J. Chem. Phys.* **1978**, *69* (11), 4921−4930.
(52) Zweier, J.; Aisen, P.; Peisach, J.; Mims, W. B. Pulsed electron paramagnetic resonance studies of the copper complexes of transferrin. *J. Biol. Chem.* **1979**, *254* (9), 3512−3515.
(53) Deligiannakis, Y.; Louloudi, M.; Hadjiliadis, N. Electron spin echo envelope modulation (ESEEM) spectroscopy as a tool to investigate the coordination environment of metal centers. *Coord. Chem. Rev.* **2000**, *204*, 1−112.
(54) Horsburgh, M. J.; Wharton, S. J.; Cox, A. G.; Ingham, E.; Peacock, S.; Foster, S. J. MntR modulates expression of the PerR regulon and superoxide resistance in *Staphylococcus aureus* through control of manganese uptake. *Mol. Microbiol.* **2002**, *44* (5), 1269−1286.
(55) Dintilhac, A.; Alloing, G.; Granadel, C.; Claverys, J.-P. Competence and virulence of *Streptococcus pneumoniae*: Adc and PsaA mutants exhibit a requirement for Zn and Mn resulting from inactivation of putative ABC metal permeases. *Mol. Microbiol.* **1997**, *25* (4), 727−739.
(56) Gribenko, A.; Mosyak, L.; Ghosh, S.; Parris, K.; Svenson, K.; Moran, J.; Chu, L.; Li, S.; Liu, T.; Woods, V. L., Jr.; Jansen, K. U.; Green, B. A.; Anderson, A. S.; Matsuka, Y. V. Three-dimensional structure and biophysical characterization of *Staphylococcus aureus* cell surface antigen−manganese transporter MntC. *J. Mol. Biol.* **2013**, *425* (18), 3429−3445.
(57) McDevitt, C. A.; Ogunniyi, A. D.; Valkov, E.; Lawrence, M. C.; Kobe, B.; McEwan, A. G.; Paton, J. C. A molecular mechanism for bacterial susceptibility to zinc. *PLoS Pathog.* **2011**, *7* (11), No. e1002357.

DOI: 10.1021/acs.inorgchem.9b00763
Inorg. Chem. 2019, 58, 13578−13590

(58) Walkup, G. K.; Burdette, S. C.; Lippard, S. J.; Tsien, R. Y. A new cell-permeable fluorescent probe for Zn^{2+}. *J. Am. Chem. Soc.* **2000**, *122* (23), 5644−5645.
(59) Forrer, J.; García-Rubio, I.; Schuhmam, R.; Tschaggelar, R.; Harmer, J. Cryogenic Q-band (35 GHz) probehead featuring large excitation microwave fields for pulse and continuous wave electron paramagnetic resonance spectroscopy: performance and applications. *J. Magn. Reson.* **2008**, *190* (2), 280−291.
(60) Mims, W. B. Pulsed endor experiments. *Proc. R. Soc. Math. Phys. Eng. Sci.* **1965**, *283* (1395), 452−457.
(61) Hassan, A. K.; Pardi, L. A.; Krzystek, J.; Sienkiewicz, A.; Goy, P.; Rohrer, M.; Brunel, L.-C. Ultrawide band multifrequency high-field EMR technique: a methodology for increasing spectroscopic information. *J. Magn. Reson.* **2000**, *142*, 300−312.
(62) Stich, T. A.; Lahiri, S.; Yeagle, G.; Dicus, M.; Brynda, M.; Gunn, A.; Aznar, C.; Derose, V. J.; Britt, R. D. Multifrequency pulsed EPR studies of biologically relevant manganese(II) complexes. *Appl. Magn. Reson.* **2007**, *31*, 321−341.
(63) Weil, J. A.; Bolton, J. R. *Electron Paramagnetic Resonance: Elementary Theory and Practical Applications*, 2nd ed.; Wiley-Interscience: Hoboken, NJ, 2007.

DOI: 10.1021/acs.inorgchem.9b00763
Inorg. Chem. 2019, 58, 13578−13590